FINAL PROJECT REPORT

Project Title: ON-LINE FUEL FAILURE MONITOR FOR FUEL TESTING AND MONITORING OF GAS COOLED VERY HIGH TEMPERATURE REACTORS

Covering Period: March 25th, 2005 through December 31st, 2009

Date of Report: April 22, 2010

Recipient: North Carolina State University
P.O. Box 7909
Department of Nuclear Engineering
Raleigh, NC 27695-7909

Award Number: DE-FC07-05ID14662 (NERI 05-54)

Subcontractors: N/A

Other Partners: N/A

Contact(s): Ayman I. Hawari
(919) 515-4598
ayman.hawari@ncsu.edu

Mohamed A. Bourham
(919) 515-7662
bourham@ncsu.edu

Project Objective: In both the prismatic and pebble bed designs of the gas cooled Very High Temperature Reactor (VHTR), the fuel is based on the concept of the TRISO microsphere. As part of the fuel development program for the VHTR in the United States, fuel failure experiments will be taking place at the Advanced Test Reactor of Idaho National Laboratory (INL). The objective of this project is to collaborate with the technical staff of INL to optimize the fuel failure monitoring system. Specifically, we will first study the option of performing the measurement using gamma-ray spectrometers that are placed along the path of the coolant flow. In addition, we will consider a system based on sampling the main flow, and collecting the appropriate fission products in an optimized signal to noise environment. In both cases, specialized instruments, measurements techniques, and data processing methods will be required to meet minimum detectable activity limits. Furthermore, the developed methods and instrumentation are expected to be applicable to on-line fuel failure monitoring of VHTRs.

Background: Very High Temperature Reactors (VHTR) utilize the TRISO microsphere as the fundamental fuel unit in the core. The TRISO microsphere (~ 1-mm diameter) is composed of a UO_2 kernel surrounded by a porous pyrolytic graphite buffer, an inner pyrolytic graphite layer, a silicon carbide (SiC) coating, and an outer pyrolytic graphite layer. The U-235 enrichment of the fuel is expected to range from 4% – 10% (higher enrichments are also being considered). The layer/coating system that surrounds the UO_2 kernel acts as the containment and main barrier against the environmental release of radioactivity. To understand better the behavior of this fuel under in-core conditions (e.g., high temperature, intense fast neutron flux, etc.), the US Department of Energy (DOE) is launching a fuel testing program that will take place at the Advanced Test Reactor (ATR) located at Idaho National Laboratory (INL). During this project North Carolina State University (NCSU) researchers will collaborate with INL staff for establishing an optimized system for fuel monitoring for the ATR tests. In addition, it is expected that the developed system and methods will be of general use for fuel failure monitoring in gas cooled VHTRs.

Summary: This project focused on understanding the phenomenon of fission gas release from TRISO fuel particles. TRISO microsphere fuel is the fundamental fuel unit for Very High Temperature Reactors (VHTR). A single TRISO particle consists of an inner kernel of uranium dioxide or uranium oxycarbide surrounded by layers of pyrolytic carbon and silicon carbide. If the silicon carbide layer fails, fission products, especially the noble fission gases Kr and Xe, will begin to escape the failed particle. The release of fission gas is usually quantified by measuring the ratio of the released activity (R) to the original birth activity (B), which is designated as the R/B ratio. In this project, relative Release-to-Birth indicators (I) are proposed as a technique for interpreting the results of TRISO irradiation experiments. By implementing a relative metric, it is possible to reduce the sensitivity of the indicators to instrumental uncertainties and variations in experimental conditions. Furthermore, to link experimental observations to physical mechanisms, atomistic simulation models were developed that can be used to examine the behavior of fission gases in the fuel matrix. In this case, classical molecular dynamics models of Uo2 were implemented and validated against published experimental data. Finally, a device for examining fission gas gamma-ray spectra in room temperature conditions was constructed and tested. It was observed that this device can provide some information. However, enhanced measurement concepts that can be implemented in in-situ release experiments may be preferable.

1. Development of Fission Gas Release Indicators

As part of the development of the Very High Temperature Reactor (VHTR) it is important to attain an understanding of the potential fission gas release from TRISO fuel. The VHTR in either its prismatic or pebble bed form is an attractive reactor design on account of its ability to produce electricity at nearly 50% thermodynamic efficiency, and the high temperature of its coolant that may be useful in the generation of Hydrogen or other process heat applications [1]. The VHTR is fuelled with TRISO particles contained in a graphite structure. In general, single TRISO particles consist of an inner kernel of uranium oxide or uranium oxycarbide surrounded by layers of pyrolytic carbon, silicon carbide, and an additional layer of pyrolytic carbon. The silicon carbide layer of TRISO particles acts as the primary barrier to the release of fission fragments into the core. In the VHTR core, TRISO fuel will be subjected to high temperature (peak around 1500 K), high radiation damage conditions (fast neutron fluence reaching $4x10^{21}$ n/cm^2), and high burn-up (15-20 % FIMA) [2]. Under these conditions, the silicon carbide layer may fail due to manufacturing defects or pressure due to fission gas build up inside the TRISO particle. If this layer fails, fission gas, most notably the noble gases Kr and Xe, will escape via different release mechanisms into the core.

There are two primary methods used to study fission gas release from different types of nuclear reactor fuel. Post Irradiation Annealing exposes fuel to a radiation field at low temperatures in order to build up fission gas without causing diffusion. The sample is then transferred into a device where it is heated to high temperatures. The fission gas is then observed as it leaves the fuel. The second major method is In-Pile Release. In this type of experiment, the fuel is irradiated in core and sweep gas flows around the fuel carrying fission products out of the core for analysis. The focus of this work is the analysis of In-Pile Release experiments for failed TRISO fuel. In this case, fission gas release from TRISO fuel is usually quantified by taking the ratio of the measured release activity (R) of a specific Kr or Xe isotope to the predicted activity of the isotope in the fuel due to irradiation conditions (i.e. birth activity (B)). This ratio is termed the Release-to-Birth Ratio (R/B). Several different semi-empirical models have been developed to predict the R/B behavior of failed TRISO particles. The different physical phenomena that contribute to the R/B ratios create distinct trends. Through proper analysis, trends in the models and trends in the experimental data can lead to a better understanding of the physical phenomena that control fission gas release from TRISO fuel.

Fission Gas Release Models

Fission gas is released from the fuel when gas migrates through the crystal structure of the fuel into the free volume between fuel grains then through the graphite matrix and into the effluent stream. The release activity due to isotopes of Krypton and Xenon that have reached equilibrium activity in the fuel can be described by R/B models. The R/B models include terms for fission product release from catastrophic failure of the TRISO particle, heavy metal contamination in the graphite matrix surrounding the fuel, and the direct recoil of fission fragments.

The major pathway for fission gas to escape the fuel and enter the effluent stream is through gaseous diffusion. Under steady state conditions, most R/B models use some form of the Booth equivalent sphere model to predict R/B caused by diffusion [3]. The Booth model can be best understood as the solution to the steady state diffusion equation for the flux of gas atoms over a sphere of fixed radius [4]. Equation (1) contains the general form of the Booth model

$$\left(\frac{R}{B}\right) = 3\sqrt{\frac{D}{\lambda a^2}}\left[\coth\left(\sqrt{\frac{\lambda a^2}{D}}\right) - \sqrt{\frac{D}{\lambda a^2}}\right], \qquad (1)$$

where D is the diffusion coefficient, λ is the decay constant, and ‘a’ is the radius of the equivalent sphere which is the fuel kernel radius for TRISO fuel. Often the D and ‘a’ terms are combined to create reduced diffusion coefficients.

The application of the Booth model is relevant to both diffusion release by the kernel and release coming from heavy metal contamination in the graphite matrix. A key feature of such models is the temperature dependent diffusion coefficients. Some models show that these coefficients may also depend on the element that is diffusing.

In this study, three different R/B models are examined. The German model [as presented in Ref. 5] uses the same form as Eq. 1 to model both gas release from the failed TRISO particle and heavy metal contamination. The JAERI model modifies this formulation to include precursor effects, burn-up corrections, and accounts for the effect of fission gas diffusion through the fuel compact matrix [6]. This model also can be used to predict R/B ratios for heavy metal contamination. The General Atomics (GA) model follows a similar approach to the other models [7], and adds terms that include recoil, thermal re-solution, and diffusion. However, this model does not contain terms for calculating release from contamination in the graphite matrix.

A major difference between the above models appears in the diffusion coefficients that were derived from different experimental measurements. Contemporary fuel tests are necessary to establish which (if any) of these models best describes the current generation of TRISO fuel. In fact, it may be necessary to combine features from the different models described above to accurately describe fission gas release.

Formulation of R/B indicators

In experimental implementation, the development of the R/B ratios involves the measurement of the activities of the radionuclides of interest using gamma-ray spectrometry. An example of this work is the Advanced Gas Reactor (AGR) TRISO fuel experiments that are currently taking place at the Advanced Test Reactor (ATR) of Idaho National Laboratory [8]. Predicted R/B ratios for the various radionuclides can be calculated using the R/B models described above and the known experimental conditions. Subsequent comparisons between model predictions and measurements can be made to infer the validity of a particular model for describing the physics of the gas release process from the fuel.

Typically, the comparison between measured R/B values and model predictions are made on an absolute basis. However, this type of comparison will include uncertainties that are contributed by both components of the ratio (R and B). The measured value of R (for a given radionuclide) represents the release activity and will include uncertainties due to statistical and instrumentation calibration factors. B is usually obtained from a neutronic model that includes a specific description of the anticipated experimental conditions. In this case, uncertainties associated with power levels (and corresponding thermal neutron fluxes) and spectral averaged cross section (e.g., for fission or for the production and loss of a given radionuclide) can be significant.

Consequently, a relative approach that could be less susceptible to such uncertainties may be preferred. Specifically, a relative R/B indicator is defined below [9]

$$I = \frac{R_1}{B_1}\left(\frac{B_2}{R_2}\right). \qquad (2)$$

In this case, 'I' (the relative indicator) is established based on the ratio of R/B values for a given radionuclide relative to the R/B value for a reference nuclide. The radionuclides of interest are the various Kr and Xe isotopes that range in half-life from minutes up to hours.

The uncertainty in 'I' will be caused by the uncertainties in R_1/R_2 and B_2/B_1. Formulating a ratio for the release rates will allow minimizing the impact of effects such as gas travel time and detector efficiency calibration [10]. The ratio of birth rates is expected to be fairly resistant to variations in irradiation conditions. This will be especially true for short-lived radionuclides that have negligible absorption cross sections [11].

Gas Release Trends Using Relative R/B Indicators

Computational Analysis

To test the approach presented above, the experimental conditions of the first in-core TRISO fuel test (AGR-1) at the ATR were used to calculate R/B ratios for the various models. Simulations of the AGR-1 experiment were performed to predict the birth activities and expected gamma ray spectrum due to failed particles and heavy metal contamination release [12]. Estimates of the birth activities of the Kr and Xe isotopes were obtained using ORIGEN [13] depletion calculations. Once the predicted R/B values were established, a reference radionuclide was chosen to create predicted relative Release-to-Birth indicators.

Figure 1 shows the predicted relative indicators (I) for failed TRISO particles using Kr-85m as the reference radionuclide versus half-life. Kr-85m was chosen as the reference isotope based on its physical properties. It has a half-life (4.48 hours) that is sufficiently short to allow reaching an equilibrium concentration in the fuel, but is long enough that decay during transport from the irradiation position to the detector is not significant. The transport time is on the order of 2 to 3 minutes [14] which poses a significant challenge for the detection of the shorter lived radionuclides of interest like Kr-90, Kr-91, and Xe-139. Kr-85m also has a distinct 75.4% yield gamma-ray at 151.2 keV that occurs in a section of the gamma ray spectrum that is relatively free of any other full energy peaks.

By recognizing the physics of a given R/B model, it is possible to observe several key trends in Fig. 1. For example, the German model is known to use a single expression to describe the diffusion coefficients of Kr and Xe for failed TRISO particles. In this case, half-life becomes the important factor in the R/B estimations showing a clear trend for the ratios to decrease as the half-life decreases.

This trend stems directly from the Booth model which is proportional to the square root of half-life for the nuclides of interest. However, in the GA model this trend is not observed. The GA model uses different empirical relationships for Kr and Xe to determine the diffusion coefficients. The

result is that this model has two separate Xe and Kr indicator trends. The JAERI model also appears to follow the same half-life trend as the German model, which is expected since the JAERI model uses only a single diffusion coefficient relationship for kernel diffusion of Kr and Xe. However, deviations from this trend are observed when examining the data for Xe-135m ($T_{1/2}$ = 15.3 min) and Xe-138 ($T_{1/2}$ = 14.1 min). This is attributed to the fact that the JAERI model accounts for the half-life of the precursor of a given isotope. In this model, the R/B for a particular nuclide is enhanced if it has a long lived precursor. Consequently, the long lived precursor of Xe-135m (I-135 $T_{1/2}$ = 6.57 h) increases its R/B when compared to a nuclide with a similar half-life like Xe-138 with a short lived precursor (I-138 $T_{1/2}$ = 6.5 s).

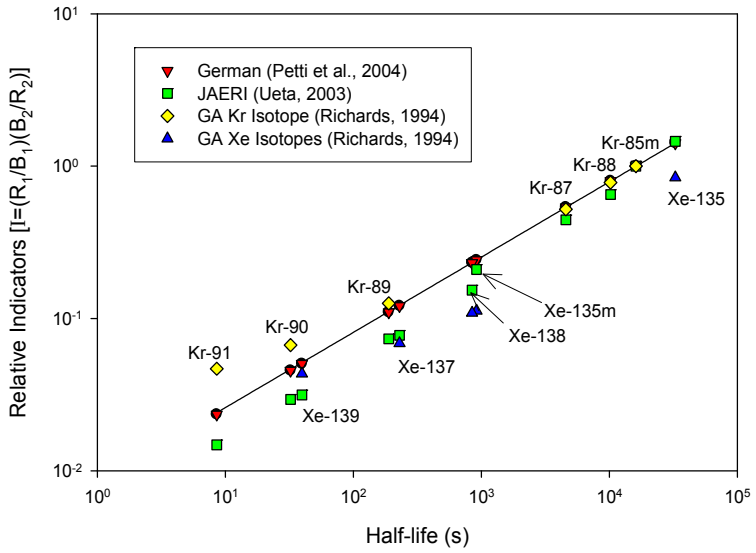

Fig. 1. Indicator values for different failure models as a function of half-life for failed TRISO particles. Kr-85m is used as the reference radionuclide and a temperature of 1448K is assumed. The solid line is used as an illustration guide to assist in the visual interpretation of the trends, but does not reflect modelling of all release mechanisms

Figure 1 also demonstrates the trends that are indicative of the second major pathway for fission gas release, i.e. direct recoil. This pathway enhances fission gas release from shorter lived isotopes that tend to decay before they can diffuse out of the fuel. Notice that the German model displays a linear relationship with half-life on the log-log plot. This is a result of ignoring recoil release. The GA and JAERI models account for recoil and do not have the strictly linear response that indicates diffusion only release mechanisms. This effect is most clearly illustrated by the indicator values of Kr-91, Kr-90, and Xe-139 for the GA model.

As seen above, it is expected that by combining the accuracy of relative R/B indicators with such observed trends for the various models, analysis of the experimental data (i.e., the gamma-ray spectra of released fission gases) can be extended to understanding, differentiating and validating the various models for fission gas release.

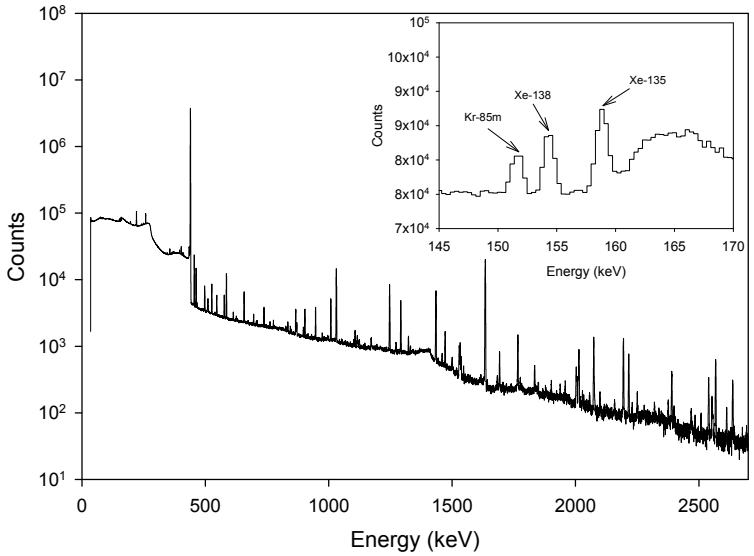

Fig. 2. AGR-1 gamma ray spectrum collected around March 28, 2007 on Capsule 2. The inset details the region of the spectrum near the 151.2 keV peak of Kr-85m [15].

Application to AGR-1 Data

As an experimental implementation of the approach presented above, an analysis was performed of a representative gamma-ray spectrum collected from the AGR-1 experiment. In this experiment, graphite fuel compacts that contain TRISO particles are irradiated at the B-10 position of the ATR. The spectrum is shown in Fig. 2 and is attributed to uranium contamination in the fuel compacts. At this time there have been no detected TRISO failures in the AGR-1 experiment [16]. High purity germanium detectors continuously collect gamma-ray spectra of the fission products exiting the AGR-1 fuel compacts. Collected spectra are periodically analyzed to attain the gamma ray peak areas. The peak areas are combined with the detector efficiency and the gamma-ray yield to derive the release activities of the isotopes of interest. Before the release activities can be transformed into Release-to-Birth indicators, they must be corrected for decay during transport from the irradiation position to the detector. For each capsule the flow rate of the He effluent is

continuously monitored and recorded at the ATR. The decay time is determined by the volume of tubing that the fission products must pass through to get to the detector divided by the volumetric flow rate of the effluent [14]. After the release activities are calculated, they are combined with the birth activities calculated from ORIGEN as show in Eq. 2 to construct the experimental relative R/B indicators.

Relative R/B indicators (I) based on the data in Fig.2 have been calculated and are shown in Fig. 3. The error bars of the experimental data are principally from counting statistics. In addition, computationally predicted relative indicators (I) based on the heavy metal contamination components of the German and JAERI models are also plotted in Fig. 3 as solid lines. The models can be displayed in this manner by assuming that the half-life of the non-reference isotope is a continuous parameter. The temperature of the fuel is assumed to be 1125 K based on AGR-1 thermocouple data [15].

There are several observations that can be ascertained from Fig. 3. The experimental data exhibits two separate trends for Kr and Xe. This behavior is qualitatively consistent with the German model, which for heavy metal contamination has two different reduced diffusion coefficient correlations for Kr and Xe. However, The German model prediction for Xe severely underestimates the magnitude the relative R/B value of Xe. This could be indicative of an inconsistency between the reduced diffusion coefficient assumed in the German model and the reduced diffusion coefficient that might be deduced from the experimental values. The experimental data suggests that the apparent difference in reduced diffusion coefficient between Kr and Xe is not as dramatic as proposed by the German model. The JAERI model has only a single trend for Kr and Xe, but it does trend closer to the experimental data than the German model predictions. This is especially true for the shorter lived isotopes like Kr-89 for which recoil release becomes an important mechanism. One feature that does not appear in Fig. 3 is evidence of a precursor effect. The experimental indicator value (I) for Xe-135m does not exhibit any enhanced diffusion due to its long lived precursor when compared to the indicator value of Xe-138.

The curvature exhibited by the JAERI model line is the result of recoil. Recoil is accounted for in the JAERI model but not in the German model for contamination. The straight lines of the German model are representative of pure diffusive release. The slope of these lines on the log-log plot is near 0.5 which corresponds to the square root of half-life dependence of the Booth model. The experimental trend lines do not have the 0.5 slope. This indicates that non-diffusive mechanisms like recoil are important for describing these experimental results.

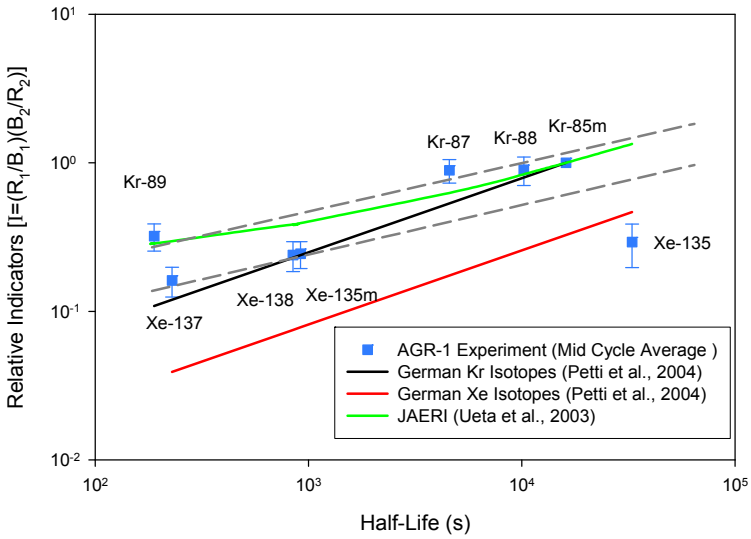

Fig. 3. A comparison between experimentally derived relative R/B Indicator (I) values and model predictions. The experimental points are based on capsule 2 measured mid-cycle data of the 2nd irradiation cycle of AGR-1. One standard deviation uncertainty bars are shown. The data was collected between March 26 and April 6, 2007. The predicted R/B indicators (shown as solid lines) are for release from heavy metal contamination at 1125K. Dashed lines are drwan through the experimental data points to assist in observing trends.

Neither model adequately describes the behavior of the Xe-135 indicator (I). This indicator is characterized by a large absorption cross section which makes its calculated B value highly sensitive to accurate knowledge of the experimental conditions and their reflection in the neutronic simulations. A modification to both the German and JAERI models is found by adjusting the loss mechanisms that are assumed in the R/B model to account for the transmutation of this radionuclide caused by its large absorption cross section. The inclusion of this correction term reduces the R/B ratio reducing the indicator values. This helps remove some of the discrepancy between experimental indicators and predicted indicators.

2. Development of Atomistic Simulations in Support of Fission Gas Release Analysis

As seen from the above analysis, in-situ irradiation testing of the fuel can provide information regarding failure mechanisms and conditions. The observable in such experiments, i.e, the gamma-ray spectra, can be used to infer the physical phenomena that determine fuel behavior. The link to predictive models of fuel behavior can be obtained by defining fundamental quantities that are in common with experiments. These quantities can be derived using atomistic simulation techniques such as molecular dynamics (MD).

The bulk or macroscopic behavior of a material is determined by the microscopic interactions of its constituent atoms. MD seeks to link the microscopic simulation of atomic systems to derive the macroscopic properties of the bulk. This is accomplished by calculating the movement of the individual atoms of a system by solving the equations of motions defined by atomic interaction potentials. Several mechanisms associated with fuel failure can be explored using different flavors of MD. These mechanisms include fission product diffusion in the crystal structure of the fuel material. In this work, the development and testing of a classical MD model for UO_2 that can be used to assists in understanding TRISO fuel failure modeling was accomplished.

Basic Properties for Uranium Dioxide for MD Simulations

Uranium Dioxide is an ionic material that has been used extensively as a fuel for light water reactors in the nuclear power industry. In addition to use in light water reactors, UO_2 has been used as the fuel kernel material in TRISO fuel for high temperature reactor designs. The uranium oxycarbide used in current generation US TRISO fuel kernels also contains a UO_2 phase. The crystal structure of UO_2 is the fluorite structure found in CaF_2. A schematic of a unit cell of the fluorite structure is shown in Fig. 4. The atomic positions seen in the unit cell picture are used to define the initial positions of atoms in a MD simulation.

For an ionic solid such as UO_2, the potential function includes short range and long range (coulomb) components to govern the interactions between atoms. There have been several UO_2 potential functions developed to simulate different physical properties. The short range potential functions tend to take on the Buckingham form shown in part A of the potential energy function shown in Eq. 3. Part B of the equation is the Coulomb portion of the potential.

$$V_{ij}\left(r_{ij}\right) = \underbrace{A_{ij}\exp\left(-\frac{r_{ij}}{\rho_{ij}}\right) - \frac{C_{ij}}{r_{ij}^{6}}}_{A} \underbrace{- \frac{1}{4\pi\varepsilon_0}\frac{Z_i Z_j}{r_{ij}}}_{B} \quad (3)$$

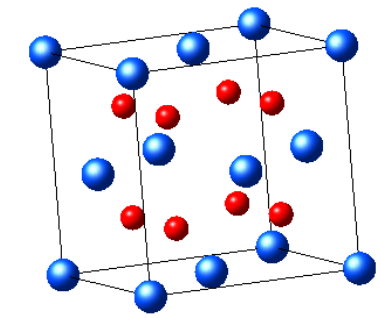

Fig. 4. The crystal structure of UO_2 (blue spheres represent U and red spheres represent O).

The potential determines the forces between two atoms 'i' and 'j' based on the distance between the two (r_{ij}). The charge on the atoms ($Z_{i,j}$) can either be formal charges (+4 for U, -2 for O), or they can be set as partial charges. However, it is important to ensure that the net charge on a UO_2 molecule is zero. The value of the potential parameters A_{ij}, ρ_{ij}, C_{ij}, and $Z_{i,j}$ can be determined by fitting to data obtained experimentally or possibly from more fundamental calculations. For example, data used in potential function validation include the thermal expansion coefficient, bulk modulus, and thermal conductivity.

Molecular Dynamics Codes

Three different Molecular Dynamics codes have been investigated for use in this research. Each code has various different benefits and weaknesses. Materials Explorer 4.0 is a commercially available MD code that incorporates a very user friendly graphical user interface in a Windows operating system [16]. While this program is a useful learning tool, its capabilities are limited. Materials Explorer lacks command line execution and input file manipulation that would allow a control script to intelligently control the execution of the code over long periods of time. Also since Materials Explorer is a commercial program the source code is not available. Modification of the source code is often necessary to derive more complex outputs from MD simulations like the heat current used in thermal conductivity calculations. Also portability of the program across several different systems (i.e. Windows, Linux, High Performance computers) is not possible without the source code. Additionally

Materials Explorer is not written to execute in parallel using several processors.

To address these concerns, the MOLDY MD code was investigated, and is now the primary MD code in use [17]. MOLDY is a general purpose MD code that is written in C. It supports many different potentials, and different potentials can be added without too much effort unlike Materials Explorer. The program can be run in all the different ensembles such as NPT, NVE and NVT. It also comes with many different ancillary programs that assist with the interpretation of the MD results. An additional MD code has also been investigated. DL_POLY is another freely available MD code developed and supported by Daresbury Laboratory in the U.K.[18]. This code has the capability of running very large systems in parallel on large computer clusters. DL_POLY_2.20 has been compiled and tested. Because of its ability to handle larger systems and installation on the NCSU High Performance Computing cluster, all larger MD systems were simulated using DL_POLY. The custom programs developed for thermal conductivity calculations are designed for MOLDY output, but could be adapted to DL_POLY output forms if necessary.

Automatic Potential Optimization with MOLDY

Once MOLDY was successfully compiled, a script was written to optimize the parameters of the Buckingham potential for UO_2. A PYTHON script was written to perform this task. The script reads in the MOLDY control file, initial positions, potential parameters, and initial test parameters. It then executes MOLDY for a set of potential parameters to be tested. The results of the run are read and compared against the real physical parameters derived from experiment.

Three parameters were fit in the initial attempt to optimize the potential. The A and ρ terms for the U-O interaction, and the charge on the U ion for all interactions. These terms can be seen in Eq. 3. This is the same strategy that was pursued by Morelon et al [19]. The justification for only modifying these three parameters follows. There is so much Coulomb repulsion between U ions that short term forces are overwhelmed, hence A, ρ, and C are not defined for the U-U interaction. In the U-O interaction, the attraction is dominated by the coulomb term, so the C term for this interaction is zero. The Morelon study found little change in the simulation by modifying the O-O interaction terms so they are not currently modified by the optimization script. In order to maintain charge neutrality, the charge on the oxygen ion must always be one half the opposite of the charge on the U ion, so the change in the O charge is always dependent on the Uranium charge.

For an initial test the potential was only optimized on the lattice constant of UO_2 at 300 K and the lattice constant at 1500 K. These temperatures span the conditions expected to be seen in the AGR tests. For each set of test parameters it was necessary to run two MD simulations under the NPT ensemble. At the conclusion of the runs, the lattice constants of the two simulations were extracted and analyzed. The initial parameters for this test were based on the Walker and Catlow potential parameters [20]. With just optimizing on the two physical properties the optimized potential was not too different from the original. The results of the optimization are shown in the Table below. In the future, the optimization control script can be expanded to other physical properties of UO_2, and other potential parameters. However the current potential produces very good results for a wide range of physical parameters.

Table 1. Results of optimizing the UO2 potential for lattice constant.

Potential Parameters

U-O A	873.9018	eV
U-O B	2.475691	$Å^{-1}$
qU	3.826355	e

Lattice Constant (Å)

	MOLDY	Experiment	% difference
300 K	5.4710	5.468	0.05456
1500 K	5.5378	5.539	0.02872

Validation of Optimized UO_2 Potential

Several different well known thermo-physical properties of UO_2 were used to validate the optimized potential function. The thermal expansion coefficient and its pressure based corollary the bulk modulus were initially used. These simpler metrics were followed by the calculation of thermal conductivity which like diffusion is a transport coefficient. The results of these validation calculations are presented in the following chapters.

Thermal Expansion

The thermal expansion of UO_2 has been examined using the optimized potential and the MOLDY code using a constant atom, pressure and temperature (NPT) ensemble. Simulations were run at 300 degree intervals for temperatures ranging from 300 to 2100 K. Each system consisted of 768 atoms run for 10 ps with 1 fs time steps. The lattice constants at each temperature were taken as the average lattice constant of the system at equilibrium. The results of the thermal expansion investigation versus literature values are shown in Fig. 5. The literature values are based on the data presented in several different experiments. The current model is able to reproduce thermal expansion over a wide

range of temperatures [21,22].

Bulk Modulus

Once a model was established for thermal expansion it was important to validate the model against other physical properties. The bulk modulus represents a material's resistance to compression under a uniform pressure and was chosen since it could be considered a pressure based corollary to thermal expansion. Eq. (4) was used to calculate the Bulk modulus by comparing the volume of the crystal at a reference pressure of 1 atm (P_1, V_1) to the volume of the crystal at much higher pressures (P_2, V_2). In general the bulk modulus should be fairly invariant under changes in pressure.

$$B = -\frac{(P_1 - P_2)}{\ln\left(V_1 / V_2\right)} \tag{4}$$

For different pressures the bulk modulus was calculated to be between 180 and 200 GPa. Experiments have found the bulk modulus to range from 179 to 207 GPa [19].

Thermal Conductivity

MD simulations were also performed to calculate the thermal conductivity of UO_2 using the Green-Kubo approach and Equilibrium Molecular Dynamics. Thermal conductivity is challenging to calculate in MD, but since it is a transport coefficient it is good test of a model's (inter-atomic potential's) ability to replicate many different transport phenomena. The thermal conductivity coefficient λ is given by the relationship shown in Equation (5) below.

$$\lambda = \frac{1}{3Vk_B T^2}\int_0^\infty dt \left\langle J(t)\, J(0)\right\rangle \tag{5}$$

Where V is the volume of the system, k_B is the Boltzmann constant, T is the temperature of the system and J(t) is the energy current, which approaches 0 as the system equilibrates. The calculation of J(t) is complicated by the need to include Coulomb forces. The energy current can be thought of as the time derivative of sum of the energy of each atom 'i' multiplied by the vector position of the ith atom.

$$\mathbf{J}(t) = \frac{d}{dt}\left[\sum_{i}^{Natms} E_i \vec{\mathbf{r}}_i\right] \tag{6}$$

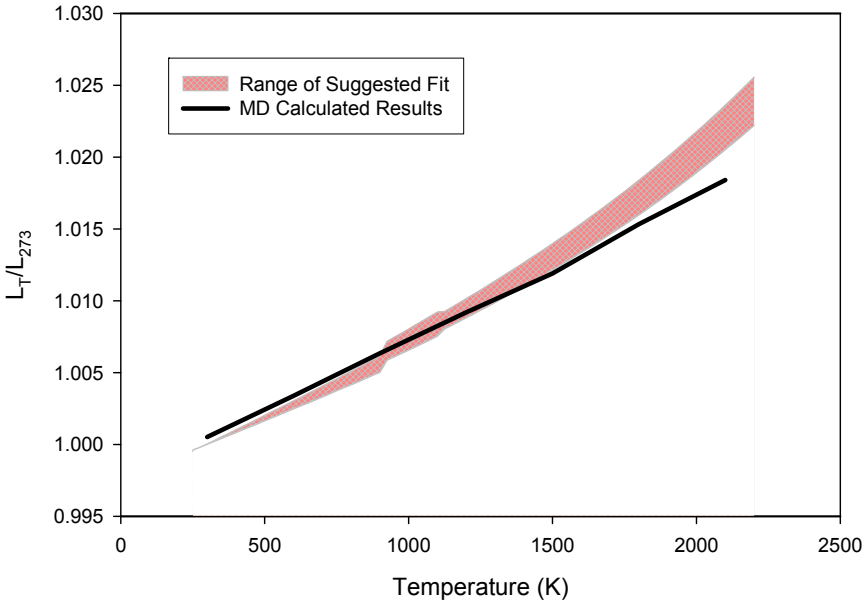

Fig. 5. Thermal Expansion of UO_2 as predicted from MD simulations.

This expression with the chain rule becomes form seen in Eq. (7) which breaks the energy current up into two convective and non-convective parts.

$$\mathbf{J}(t) = \underbrace{\sum_{i}^{Natms}\left(T_i + U_i - \hat{E}_i\right)\vec{v}_i}_{\text{Convective Term}} + \underbrace{\sum_{i}^{Natms}\vec{v}_i\vec{F}_i\vec{r}_i}_{\text{Non-Convective Term}} \tag{7}$$

The kinetic energy term for each atom (T_i) is easily calculated from the velocity of each individual atom in the system. The potential energy for each atom is calculated from a combination of sources including the short range interactions from the problem specific inter-atomic potentials, the real space part of the Ewald sums, and the reciprocal space terms of the Ewald sums that are used to calculate the coulomb interactions. The short range interactions combined with the real space part of the Ewald sum can be quickly calculated. The reciprocal or Fourier space Ewald sums require more computation and are found from the following equation.

$$U_{reciprocal} = \underbrace{\frac{1}{\varepsilon_0 V}\sum_{k>0}\frac{1}{k^2}e^{-\frac{k^2}{4\alpha^2}}\left\{\left|\sum_{i=1}^{N} q_i \cos\left(k\square r_i\right)\right|^2 + \left|\sum_{i=1}^{N} q_i \sin\left(k\square r_i\right)\right|^2\right\}}_{\text{Fourier Space Term}} - \underbrace{\frac{\alpha}{4\pi^{\frac{3}{2}}\varepsilon_0}\sum_{i=1}^{N} q_i^2}_{\text{Self-Energy Term}} \qquad (8)$$

In Equation (8), ε_0 is the electric constant, V is the volume of the simulation cell, k is the reciprocal vector of the simulation unit cell, α is a convergence factor for the Ewald sum, N is the number of atoms in a system, and q_i is the charge on atom i in the system. The equation also contains a self-energy term to account for energy contribution from the charge on the individual atoms.

The non-convective term of the energy density is computationally expensive to compute due to the need to calculate the force from every atomic interaction in the system. Additionally, calculation of this term requires combining the force and the position of each atom into a tensor (S_{ab}). The detailed equations for this term are shown in Equations (9) and (10).

$$\mathbf{J}\left(t\right)_{Non-Convective} = \sum_{i}^{Natms}\sum_{j}^{Natms}\vec{v}_i\vec{F}_{ij}\vec{\mathbf{r}}_i = \sum_{i=1}^{N}\mathbf{v_i}\begin{pmatrix} S_{xx} & S_{xy} & S_{xz} \\ S_{yx} & S_{yy} & S_{yz} \\ S_{zx} & S_{zy} & S_{zz} \end{pmatrix}, \qquad (9)$$

Where

$$S_{ab} = \frac{1}{2}\sum_{j\neq i}^{Natoms}\frac{a_{ij}b_{ij}}{\left|\mathbf{r}_{ij}\right|^2}\left[\begin{array}{l} \underbrace{F\left(r_{ij}\right)}_{\text{short range}} + \underbrace{\frac{1}{4\pi\varepsilon_0}q_i q_j\left(\frac{erfc\left(\alpha\left|\mathbf{r}_{ij}\right|\right)}{\left|\mathbf{r}_{ij}\right|} + \frac{2\alpha}{\sqrt{\pi}}e^{-\alpha^2\left|\mathbf{r}_{ij}\right|^2}\right)}_{\text{real space Coulombic}} - \cdots \\ \cdots - \underbrace{\frac{1}{4\pi\varepsilon_0}q_i\sum_{\mathbf{k}}\frac{k_a}{\left|\mathbf{k}\right|}\frac{k_b}{\left|\mathbf{k}\right|}\frac{4\pi e^{-\left|\mathbf{k}\right|^2/4\alpha^2}}{\left|\mathbf{k}\right|^2}\left(1+\frac{\left|\mathbf{k}\right|^2}{4\alpha^2}\right)}_{\text{reciprocal space Coulombic}}\times\cdots \\ \underbrace{\cdots\times\left(\cos\left(\mathbf{k}\square\mathbf{r}_i\right)\sum_{j=1}^{Natoms}q_j\sin\left(\mathbf{k}\square\mathbf{r}_j\right) - \sin\left(\mathbf{k}\square\mathbf{r}_i\right)\sum_{j=1}^{Natoms}q_j\cos\left(\mathbf{k}\square\mathbf{r}_j\right)\right)}_{\text{reciprocal space Coulombic}} \end{array}\right] \qquad (10)$$

The S tensor is defined by the atomic positions, and the forces due to the

Coulomb and short range potentials [23]. The term $F(r_{ij})$ represents the forces due to the short range inter-atomic potentials. In the equation for the tensor, the a and b terms are the x, y, z terms for the tensor that come from the x, y, z components of the r_{ij} vector between atoms i and j. The $k_{a,b}$ terms are the x, y, z componets of the reciprocal lattice vector of the MD cell.

In addition, the reciprocal lattice vector is understood to be defined as

$$k_x = 2\pi \frac{a_y \times a_z}{a_x \cdot a_y \times a_z};\ k_y = 2\pi \frac{a_z \times a_x}{a_x \cdot a_y \times a_z};\ k_z = 2\pi \frac{a_x \times a_y}{a_x \cdot a_y \times a_z}, \qquad (11)$$

where $a_{x,y,z}$ is the real space lattice vector of the MD cell.

Calculating the heat current is a complex process, and a program was written to process the outputs of MOLDY simulations for this task. After extensive testing which included benchmarking against Ar thermal conductivity simulations, UO_2 thermal conductivity results were produced. Simulations were performed with the optimized potential that is loosely based on the Walker-Catlow potential. The simulation time for each temperature was 10 ps with 1 fs time steps, and both NPT and NVT ensemble results were produced. The results of the simulations are shown in Fig. 6 for the NPT ensemble and Fig. 7 for the NVT ensemble. The Calculations are compared to a suggested value fit of several different published sets of experimental data [24] and against the experimental results of Bates [25]. The calculated thermal conductivity values agree well with the experimental data. These results suggest that UO_2 behavior is being reasonably simulated by the current model.

Finally, it should be noted that thermal conductivity is a transport coefficient that is well known and has an abundance of experimental data to benchmark against. This is particularly useful, since the goal of further simulations is to examine the diffusion of noble gas fission products. Diffusion is another transport process, but it does not have a large library of experimental data. With the model benchmarked against thermal conductivity it should now be possible to begin looking into the diffusion mechanisms for noble gas fission products (Kr, Xe). The starting point in this case would be the MD potentials that describe the interaction between UO_2 and the noble gases (Kr and Xe).

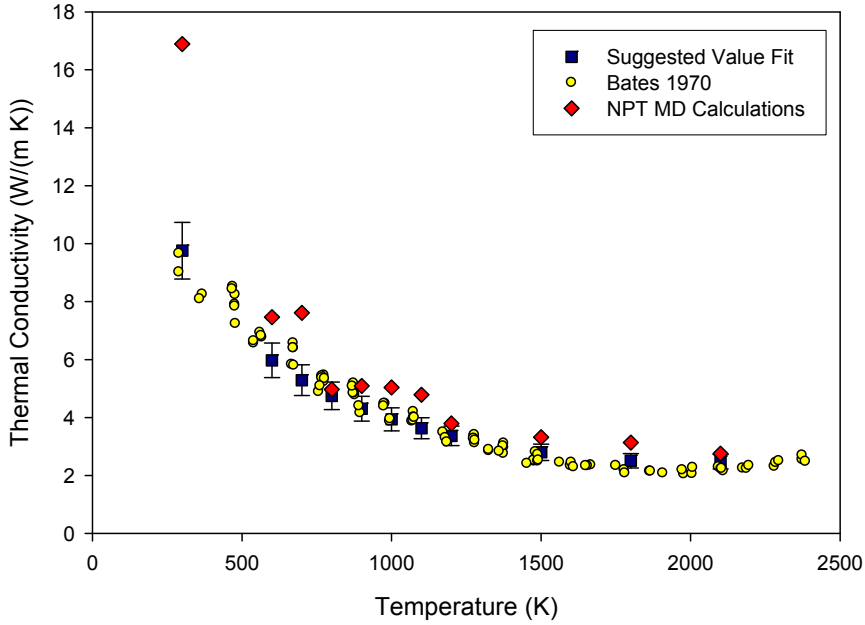

Fig. 6. Thermal Conductivity Calculations for NPT Ensemble with Experimental Data and a suggested fit to several sets of Experimental Data.

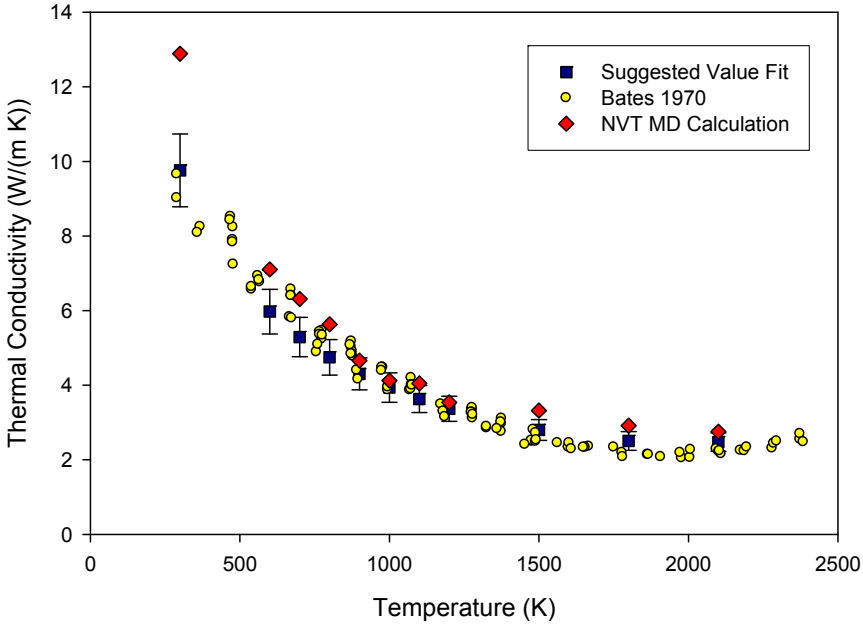

Fig. 7. Thermal Conductivity Calculations for NVT Ensemble with Experimental Data and a suggested fit to several sets of Experimental Data.

3. Evaluation of an Approach for Room Temperature Gamma-Ray Spectrometry Using Isotopic Separation

During this project a scheme was examined for isolating the Kr and Xe fission gases that may be released during a fuel irradiation experiment and detecting their gamma-ray signatures. This scheme is based on a device that is designed to ionize a sample of the flow gas and to magnetically and selectively steer the targeted gas species towards the gamma-ray detector.

The front and top view of the test device can be seen in Figures 8 and 9. Gas enters the glass 'T' section where the electrodes create an inductive plasma. The electrodes were connected to a transformer that amplified the peak-to-peak voltage of an AC power source 1000x, and the signal was 180^{o} out of phase between the two electrodes. The magnets consisted of two identically wound coils placed directly above the centerline of the glass 'T' tube. The current for the magnet was supplied by a 60 V, 20 A, DC power supply. The magnets direct the ionized plasma around the elbow of the glass and towards the detector. A pressure gauge located upstream from the inlet is used to determine when the device has reached a low enough pressure to generate plasma. The detector used in this work is a 1.5 x 1.5 inch LaBr(Ce) scintillator. It is collimated as much as possible by lead bricks and is located inside a magnetic shield that prevents interference from the electromagnets of the device. The magnetic field of the device was distorting the energy calibration of the detector. The detector is mounted at an angle looking down on the area just below the elbow of the glass 'T'. This put the detector out of the direct line of sight to the main plasma channel and allows it to preferentially detect magnetically steered plasma.

Radioactive samples of Kr and Xe are created with neutron activation in the NCSU Pulstar reactor. Natural Kr and Xe are used as the activation sample for these tests. Both Kr and Xe have several stable isotopes that lead to many different activation products. However, only Kr-85m and Xe-125 are created in sufficient activity and have a half life long enough to be useful in these tests. Samples of gas are heat sealed in 7 mL vials and shot into the reactor using the pneumatic rabbit system for irradiation times of usually 10 to 20 minutes depending on the needs of the sample and the operating power of the reactor. Since the samples are of finite size, the plasma device is operated as a closed system for radioactive tests meaning the valve to the main vacuum pump is closed during radioactive gas operation. In this configuration the plasma device can operate for several hours given its leak rate of approximately 0.5 torr per hour. Closed system operation is also necessary from a radiological safety standpoint given the ALARA principle.

A radioactive sample transfer device was assembled to provide for the easy insertion of the radioactive samples into the system. The transfer device is shown in Fig. 10. This device connects to the vacuum system and has flexible tubing to allow for the crushing of the sample vial to release the gas.

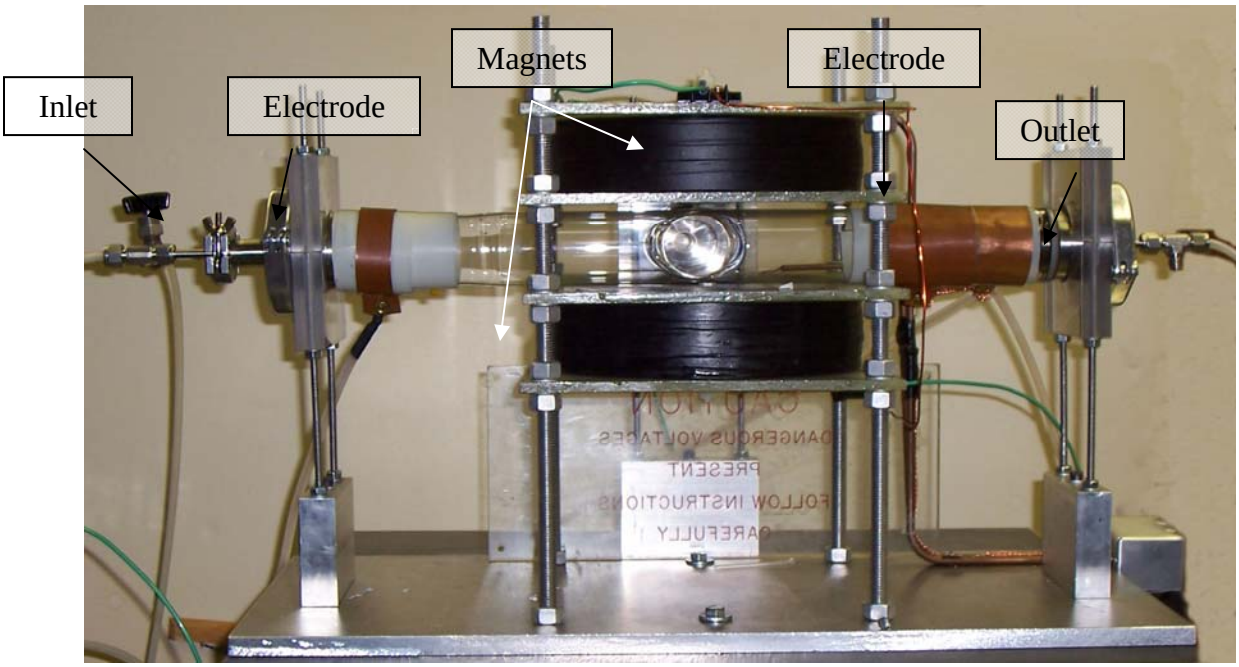

Fig. 8. Front View of the Separation Device Prototype.

Operational Characteristics of Separation Test Cell

During operation of the device, the system is first purged with He and then pumped down to a pressure of about 1.75 torr. Once the sample vial is crushed the radioactive sample fills the system up to a total pressure of about 4 torr. A plasma is then established and counts are collected on the detector system for various different magnetic settings. The counting time for each magnetic setting is dependent on the activity sample. Usually adequate counting statistics (~1%) are collected after 5 or 10 minutes of counting. Measurements have been taken at approximately 30 or 60 Gauss increments up to a maximum magnetic field of about 537 G. The results of this measurement are shown in Fig. 11. The two coils have a resistance of 3.3 Ohms each. They are wired in parallel to reduce the effective resistance resulting in half the total power supply current flowing through each coil. The LaBr(Ce) detector used in this experiment can easily distinguish between the 4 primary gamma-rays emitted by Kr-

85m (151 and 302 keV) and Xe-125 (188 and 243 keV). A sample spectrum that contains both Kr-85m peaks and Xe-125 peaks is shown in Fig. 12. Peak areas are recorded by the MCA software and then post processed to account for source decay. Experimental uncertainty is assigned based on counting statistics and standard error propagation techniques.

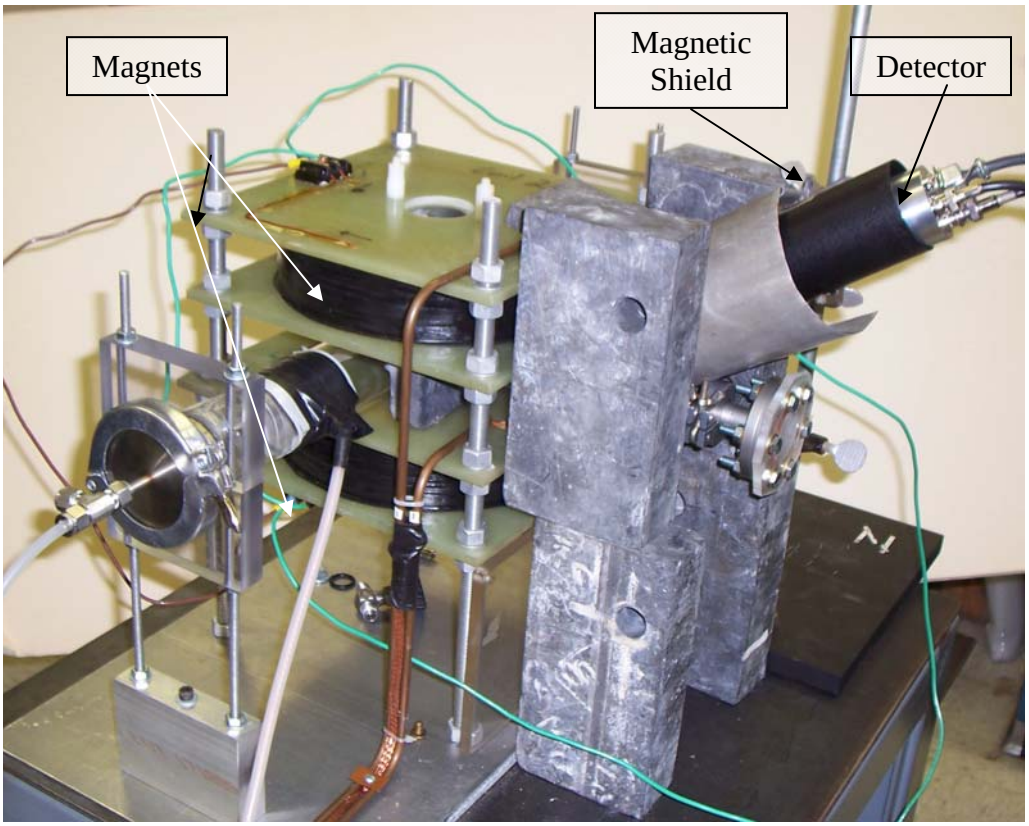

Fig. 9. Plasma Device Prototype with LaBr(Ce) detector and shielding.

Fig. 10. Radioactive Sample Transfer device with Xe-3 sample inside.

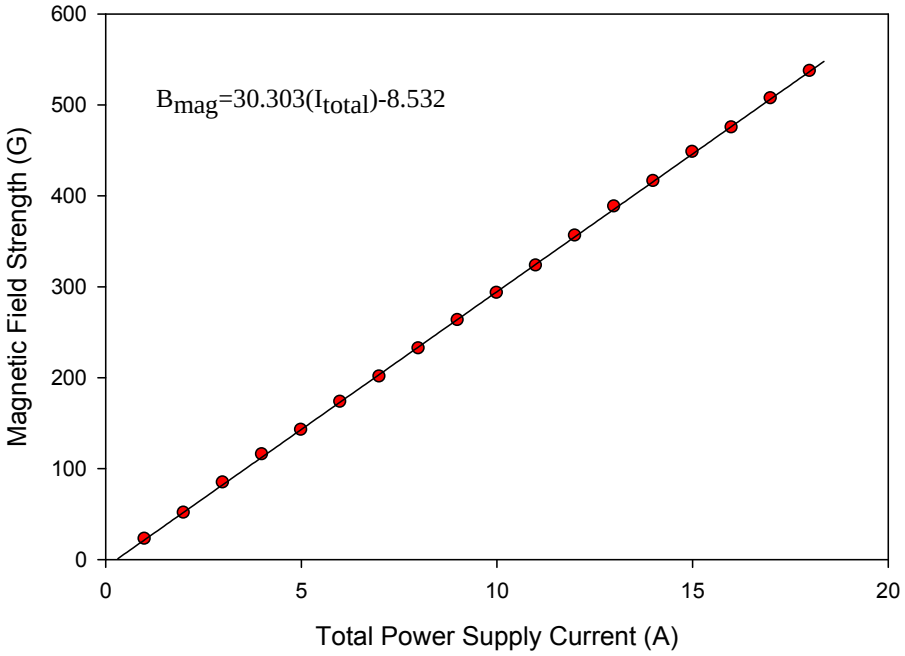

Fig. 11. Measured relationship between Total Power Supply Current and Magnetic Field Strength for case where coils are wired in parallel and linear fit to this relationship.

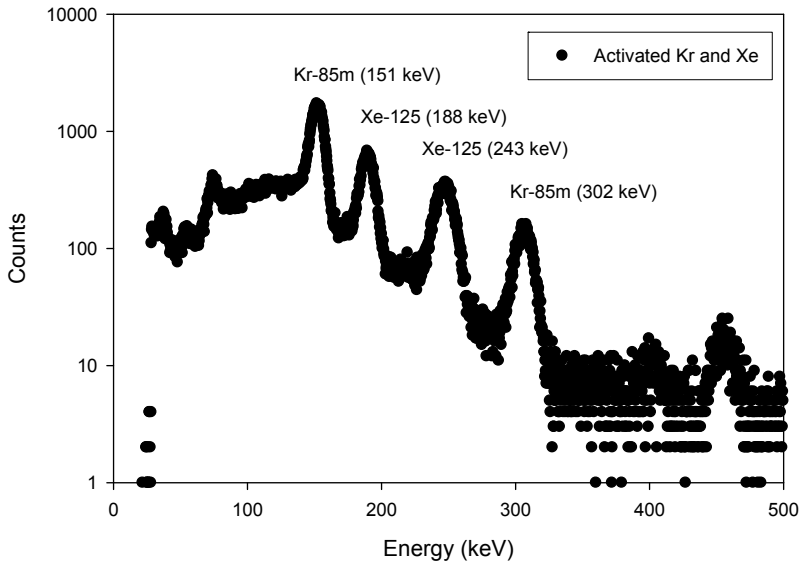

Fig. 12. A Sample Spectrum of Kr-85m and Xe-125 on the LaBr(Ce) Detector Results from Plasma Separation Test Cell

The test cell underwent several different modifications each of which lead to a better understanding of the physics occurring inside the device. Initial tests illustrated the need to modify the device in several key ways. First a magnetic shield for the detector was added to eliminate the interaction of the electrons in the PM-tube and detector crystal with the magnetic field from the device's Hemholtz coils. Shielding was also added to the device and around the detector to limit the gamma source to nuclei decaying in the center and 3rd leg of the glass T. Additionally the detector was moved from viewing the device straight down the 3rd leg to viewing the 3rd leg at an angle looking down onto the device as is shown in Fig. 9. Improvements were also made in the preparation of the Kr and Xe gas samples that were irradiated in the reactor. The samples were filled by what will be called the "Glove Method" that lead to more consistent sample preparations and less noble gas waste. In this process the 7mL sample vials used for irradiation are placed inside a nitrile examination glove with most of the air removed. The glove is then filled like a balloon with either Kr or Xe. The samples are then closed while inside noble gas atmosphere of the glove then removed and heat sealed for irradiation. After these improvements were made tests were performed that successfully demonstrated a statistically significant change in the gamma source strength with respect to changing the magnetic field.

Several different tests were performed to evaluate the device performance in two key areas. The first was the relationship between magnetic field strength and a change in counts or effective source strength observed by the detector, and the second was the ability of the device to selectively enhance either the Kr or the Xe component of the signal. Typically, counts were taken for long enough to adequately establish good counting statistics (<1% relative error) in at least the lower energy Kr-85m and Xe-125 peaks at different magnetic field settings. The frequency setting on the power supply was adjusted to shape the plasma in the glass 'T' into a coherent cylinder usually in the range 15-25 kHz. This setting was left unchanged for the duration of each test that consisted of sweeping through the magnetic field intensity range.

The initial results of the performed tests are shown in Fig. 13. Kr and Xe were separately injected into the device and the change in the relative source strength as a function of magnetic field strength was measured. The initial tests were limited to about 425 G because of the voltage limits of the magnetic power supply. In subsequent tests the coils that made up the magnet were wired in parallel instead of in series, this modification allowed a larger range of magnetic field strengths to be explored as can be seen in Figures 14 and 15. However the larger range did not lead to a

greater enhancement in the relative source strength at the detector. It appeared that the change in effective source strength reached a threshold above about 400 G where any additional enhancement from the magnetic field was offset by competing physical phenomena. The threshold is very clear in the Kr only data shown in Fig. 16. However, both Kr and Xe develop the roughly the same enhancement in source strength at the same magnetic fields.

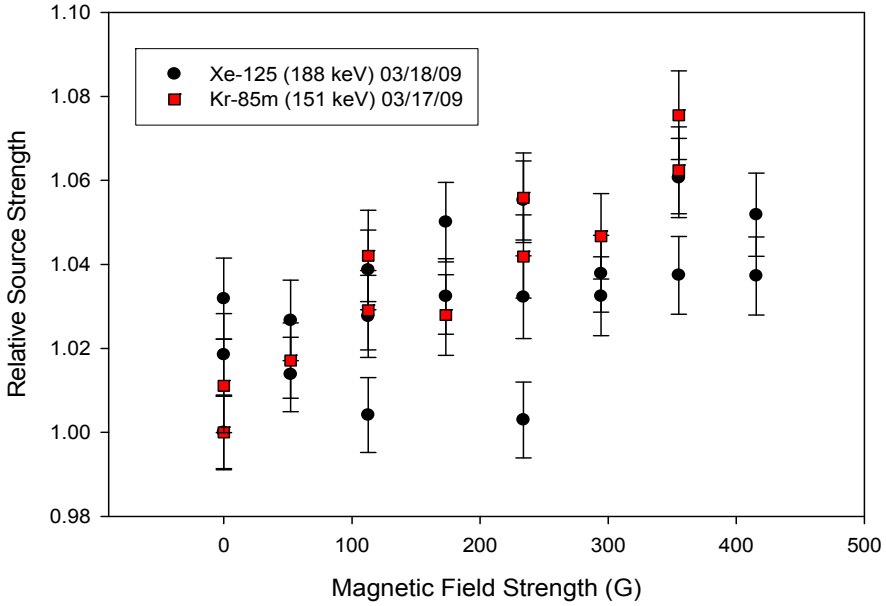

Fig. 13. Separate Kr and Xe Measurements of signal enhancement versus magnetic field strength.

From these results it can be concluded that some change in the relative source strength of the samples being tested in the device is occurring with respect to magnetic field strength. Evidence of separation of the Kr and Xe species was not observed in these tests. However, the concept does show promise in enhancing the results of in-core fueled experiments. There are several conditions that could not be tested with the current equipment, but could potentially enhance the performance of a similar device. The creation of a consistent flow for all gas in the device would improve the ability of the magnetic field to separate the Kr and Xe ions. Lowering the pressure would also be ideal however lowering the pressure must be balanced against supplying enough radioactive material to the detector to allow for detection.

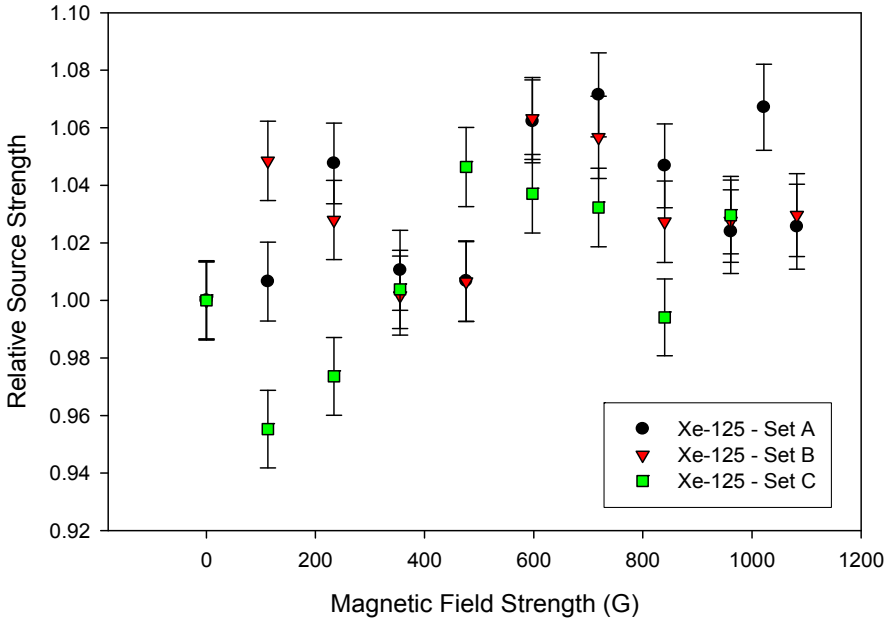

Fig. 14. Xe Measurements of signal enhancement vs. magnetic field strength over a larger range of magnetic field strength.

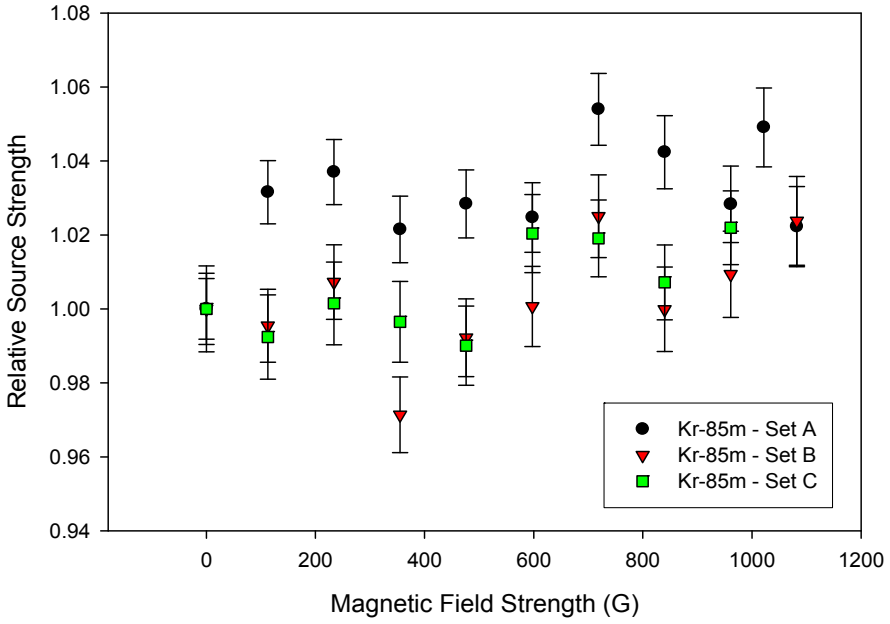

Fig. 15. Kr Measurements of signal enhancement vs. magnetic field strength over a larger range of magnetic field strength.

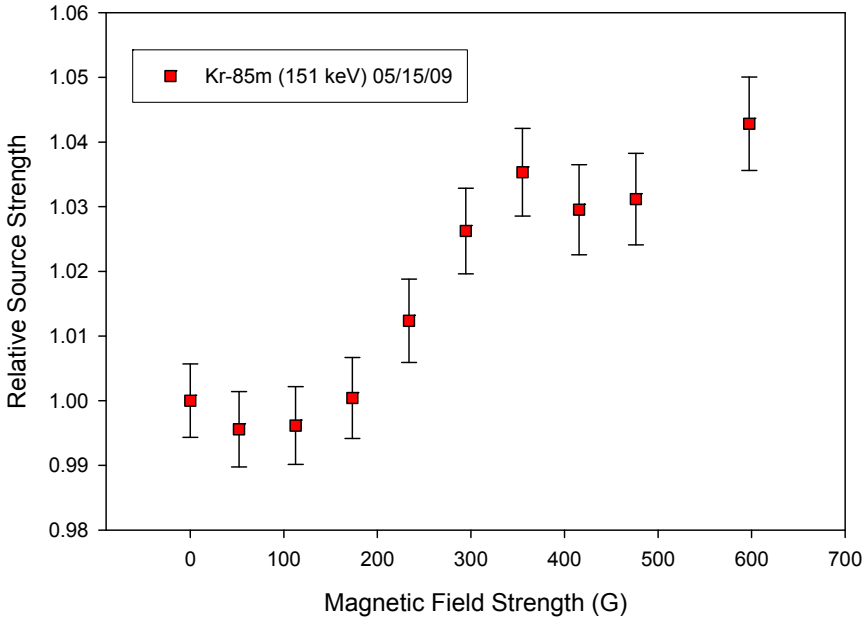

Fig. 16. Kr only measurement of source strength vs. magnetic field.

For future work, an alternative design has been considered that involves sampling a small amount of gas and then ionizing it all at a single point then injecting the ions into a 1x1 m vacuum chamber. Inside the chamber orthogonal DC electric and magnetic fields would create separation of the Kr and Xe much more completely than is possible in the current system. This system would also be operated at a much lower pressure to lessen the possibility of ion recombination. All these physics driven design features should allow for a more clear elemental separation.

References

1) LaBar, M.P., 2002. The Gas Turbine – Modular Helium Reactor: A Promising Option for Near Term Deployment, GA-A23952, General Atomics.
2) Maki, J.T., Petti, D.A., Knudson, D.L., Miller, G.K., 2007. The challenges associated with high burnup, high temperature and accelerated irradiation for TRISO-coated particle fuel, J. Nuclear Materials. 371, p. 270-280.
3) Booth, A. H., 1957. A Method for Calculating Fission Gas Diffusion from UO2 Fuel and its Application to the X-2-F Loop Test. Report CRDC-721, Atomic Energy of Canada Limited.
4) Olander D. R., 1976. Fundamental Aspects of Nuclear Reactor Fuel Elements, TID-26711-P1, U.S ERDA Technical Information Center.
5) Petti, D.A., Martin, P., Phelip, M., Ballinger, R., 2004. Development of Improved Models and Designs for Coated-Particle Gas Reactor Fuels, INEEL/EXT-05-02615.
6) Ueta, S., Sumita J., Emori, K., Takahashi, M., Sawa, K., 2003. Fuel and Fission Gas Behavior during Riste-to-Power Test of the High Temperature Engineering Test Reactor (HTTR), J. of Nuclear Science and Technology, Vol 40, p. 679-686.
7) Richards, M. B., 1994. Fission-Gas Release from UCO Microspheres: A Theoretical Model for Fractional Release from Non-hydrolyzed Fuel with Model Parameters Derived from Capsule HFR-B1 Data, General Atomics Report 818:MBR:001:94.
8) Petti, D.A., Gougar, H., Bell, G.L., 2005. The DOE Advanced Gas Reactor (AGR) Fuel Development and Qualification Program. Conference: 2005 International Congress on Advances in Nuclear Power Plants, INEEL/CON-04-02416, OSTI ID: 911109.
9) Harp, J.M., Hawari, A.I., 2007. Investigating TRISO Fuel Fission Gas Release Models Using Relative Release-to-Birth Indicators, Trans. American Nuclear Society, 96, p 365-367.
10) Hawari, A.I., Fleming, R.F., 1994. High accuracy determination of the shape of the efficiency curve of the HPGe detector in the energy range 900 to 1300 keV, Nuclear Instruments and Methods in Physics Research-A, v. 353, p. 106-108.
11) Harp, J.M., 2007. Investigation of Failed TRISO Fuel Assay Using Gamma-Ray Spectrometry, M.S. Thesis, North Carolina State University.
12) Harp, J.M., Hawari, A.I., Bourham, M.A., 2007. Simulation of Gamma-Ray Spectrometry of Failed TRISO Fuel, Nuclear Instruments and Methods in Physics Research-A, v. 579, p. 301-304.
13) Croff, A.G. 1980. ORIGEN: Isotope Generation and Depletion Code System Matrix Exponential Method, Version 2.2. Oak Ridge National Laboratory, ORNL/TM-7175.

14) Hartwell, J.K., Walter, J.B., Scates, D.M., Drigert M.W., 2007. Determination Of The AGR-1 Capsule to FPMS Spectrometer Transport Volumes From Leadout Flow Test Data, INL/EXT-07-12494.
15) Hartwell, J.K., 2007b. private communication.
16) Fujitsu Limited, Materials Explorer Ultra 4.0, 2006.
17) K. Refson, “Moldy: a portable molecular dynamics simulation program for serial and parallel computers,” Computer Physics Communications, 126(3):309--328, 2000.
18) W Smith, T.R. Forester, “DL_POLY 2.0. A General Purpose Parallel Molecular Dynamics Package,” J. Mol. Graphics, 1996.
19) N.D. Morelon, D. Ghaleb, J.M. Delaye, L. Van Brutzel, Philosophical Magazine, v. 83, n. 13, 1533-1550, 2003.
20) J.R. Walker, C.R.A. Catlow, “Structural and Dynamic Properties of UO2 at high temperatures,” J. Phys. C: Solid State Phys., vol. 14, p.979-983, (1981).
21) J. K. Fink, “Thermophysical properties of uranium dioxide,” J. Nuclear Materials, vol. 279, p. 1-18, (2000).
22) J. K. Fink, International Nuclear Safety Center Documentation, http://www.insc.anl.gov/.
23) S. Motoyama, Y. Ichikawa, Y. Hiwatari, “Thermal conductivity of uranium dioxide by nonequilibrium molecular dynamics simulation,” Physical Review B, v. 60, n. 1, 1999.
24) J. K. Fink, “Thermophysical properties of uranium dioxide,” J. Nuclear Materials, vol. 279, p. 1-18, (2000).
25) J.L. Bates, High-temperature thermal conductivity of round robin' uranium dioxide, Battelle Memorial Institute Pacific Northwest Laboratories Report BNWL-1431, 1970.

Related Publications

Several publications related to this project were produced:

1) J. M. Harp, Ayman I. Hawari, "Application of Relative Release-To-Birth Indicators for Investigating TRISO Fuel Fission Gas Release Models," PHYSOR-2008: International Conference on the Physics of Reactors, Nuclear Power: A Sustainable Resource, Interlaken, Switzerland, 2008.

2) J. M. Harp, Ayman I. Hawari, "Development of Molecular Dynamics Models for Simulating TRISO Fuel Kernels," Embedded Topical Meeting on Nuclear Fuels and Structural Materials for the Next Generation Nuclear Reactors, Anaheim, CA, 2008.

3) J. M. Harp, Ayman I. Hawari, M. A. Bourham, "Simulation of gamma-ray spectrometry of failed TRISO fuel," *Nuclear Instruments and Methods in Physics Research A*, 579, 301, 2007.

4) J. M. Harp, Ayman I. Hawari, "Investigating TRISO Fuel Fission Gas Release Models Using Relative Release-To-Birth Indicators," *Transactions of the American Nuclear Society*, 96, 2007.

5) J. M. Harp, E. H. Martin, Ayman I. Hawari, M. A. Bourham, "Studying TRISO Fuel Failure Using Passive Gamma-Ray Spectrometry," Embedded Topical Meeting on Nuclear Fuels and Structural Materials for the Next Generation Nuclear Reactors, Reno, NV, 2006.

Milestone Status Table:

Phase 1

ID Number	Task / Milestone Description	Planned Completion	Actual Completion	Comments
(a)	Communicate with INL staff and obtain information on the experimental conditions (irradiation geometry, neutron energy spectrum, temperature, etc.) for capsule irradiations at the ATR. Based on this information construct MCNP/MONTEBURNS/ORIGEN models for calculation of the isotopics of irradiated compacts and TRISO microspheres as a function of irradiation time	03/31/2006	03/31/2006	
(b)	Use the isotopics information combined with details on possible release models to estimate the gamma-ray source structure at the detection locations. Construct the source and simulate the response of various detectors (HPGe, CZT, HPXe, La halide detectors, etc.) that may be directly viewing the effluent stream. Take into account plate-out and count rate effects in the simulation and produce detector pulse height spectra with and without random summing effects. Perform the same analysis for a sample extracted from the effluent stream. Consult with INL staff to ensure the accuracy of any estimates we make	03/31/2006	03/31/2006	
(c)	Use the SIMION code system to design and optimize the charged particle guide portion of the gas extraction system	03/31/2006	03/31/2006	
(d)	Acquire the needed equipment and detectors to build the gas extraction and analysis system	03/31/2006	03/31/2006	
(e)	Produce a preliminary version of the gas extraction and analysis system	03/31/2006	03/31/2006	

Phase 2

ID Number	Task / Milestone Description	Planned Completion	Actual Completion	Comments
(a)	Explore various methods of spectral analysis that are suited for low resolution room temperature detectors.	03/31/2007	03/31/2007	
(b)	Setup the MDA limits for the various detection approaches: using various detectors that view the main the effluent stream, and using the same detectors to view and analyze an extracted effluent stream.	03/31/2007	03/31/2007	
(c)	Consult with INL staff regarding the findings and how they can be incorporated into the fuel testing program at the ATR.	03/31/2007	03/31/2007	
(d)	Test the gas extraction system using non-radioactive Xe and Kr gas to verify its mass analyzing capabilities.	03/31/2007	03/31/2007	
(e)	Perform an experiment to test the extraction and detection capabilities of the gas extraction and analysis system.	03/31/2007	03/31/2007	

Phase 3

ID Number	Task / Milestone Description	Planned Completion	Actual Completion	Comments
(a)	Work with INL staff to optimize the detection system, methods and procedures in relation to R/B information and the connection of this information to mechanistic failure models.	05/31/2009	05/31/2009	
(b)	Work with INL staff to implement the findings of this project on the ground at the ATR (e.g., the double-ratio method).	05/31/2009	12/31/2009	
(c)	If the gas extraction and analysis system proves to be the best approach for fuel failure monitoring, deliver a prototype device to INL for testing at the ATR.	05/31/2009	12/31/2009	

Budget Data (12/31/2009):

NC State University			Approved Spending Plan			Actual Spent to Date		
Phase / Budget Period			DOE Amount	Cost Share	Total	DOE Amount	Cost Share	Total
	From	To						
Phase 1	03/25/05	03/24/06	$183,140	---	$183,140	$68,461.67	---	$68,461.67
Phase 2	03/25/06	03/24/07	$166,079	---	$166,079	$176,899.79	---	$176,899.79
Phase 3	03/24/07	12/31/09	$149,210	---	$149,210	$253,067.54	---	$253,067.54
		Totals	$498,429	---	$498,429	$498,429	---	$498,429